Analysis of TerraSAR-X data sensitivity to bare soil moisture, roughness, composition and soil crust

M. Aubert, N. Baghdadi, M. Zribi, A. Douaoui, C. Loumagne, F. Baup, M. El Hajj, Sébastien Garrigues

1   # Characterization of the soil surface by TerraSAR-X imagery

2

3   **M. Aubert[1], N. Baghdadi[1], M. Zribi[2], A. Douaoui[3], C. Loumagne[4], F. Baup[2], M. El Hajj[5], S. Garrigues[6]**

4

5   [1]*CEMAGREF – UMR TETIS, 34196 Montpellier (France), Email: nicolas.baghdadi@teledetection.fr; maelle.aubert@teledetection.fr, tel : + 33 4*

6   *67 54 87 07*

7   [2]*CESBIO, 31401 Toulouse (France), Email : Mehrez.Zribi@latmos.ipsl.fr; frederic.baup@cesbio.cnes.fr*

8   [3]*Laboratoire Eau, roche et plante, Centre univeristaire de Khémis miliana, 44225 (Algérie), Email : abdouaoui@yahoo.fr*

9   [4]*CEMAGREF – UR HBAN, 92163 Antony (France), Email : cecile.loumagne@cemagref.fr*

10   [5]*NOVELTIS, 31520 Ramonville-Saint Agne (France), Email : mahmoud.elhajj@noveltis.fr*

11   [6]*CNES, 31000 Toulouse (France), Email: sebastien.garrigues@cnes.fr*

12

13   **Corresponding author:**

14   Maëlle Aubert

15   500 rue Jean-François Breton, 34093 Montpellier Cedex 5, France

16   Tel : +33 4.67.54.87.54

17   Fax: +33 4.67.54.87.00 (France)

18   Email : maelle.aubert@teledetection.fr

19

20

20   **ABSTRACT**

21   Soils play a key role in shaping the environment and in risk assessment. We characterized the soils

22   of bare agricultural plots using TerraSAR-X (9.5 GHz) data acquired in 2009 and 2010. We

23   analyzed the behavior of the TerraSAR-X signal for two configurations, HH-25° and HH-50°, with

24   regard to several soil conditions: moisture content, surface roughness, soil composition and soil-

25   surface structure (slaking crust).

26   The TerraSAR-X signal was more sensitive to soil moisture at a low (25°) incidence angle than at

27   a high incidence angle (50°). For high soil moisture (>25%), the TerraSAR-X signal was more

28   sensitive to soil roughness at a high incidence angle (50°) than at a low incidence angle (25°).

29   The high spatial resolution of the TerraSAR-X data (1 m) enabled the soil composition and slaking

30   crust to be analyzed at the within-plot scale based on the radar signal. The two loamy-soil

31   categories that composed our training plots did not differ sufficiently in their percentages of sand

32   and clay to be discriminated by the X-band radar signal.

33   However, the TerraSAR-X signal has the potential to detect low variations of soil moisture at the

34   within-plot scale. Consequently, the spatial distribution of slaking crust could be detected when

35   soil moisture variation is observed between soil crusted and soil without crust. Indeed, areas

36   covered by slaking crust could have greater soil moisture and consequently a greater

37   backscattering signal than soils without crust.

38

39   ***Keywords:*** *soil moisture, roughness, soil composition, slaking crust, X-band, TerraSAR-X images,*
40   *within field plot scale.*

41

42

42 ## 1. INTRODUCTION

43 Floods, drought and erosion are major issues for risk assessment. In the context of sustainable

44 development, soil management is important for environmental and socioeconomic applications.

45 Hence, there is a need for continuous information about key soil parameters to predict and

46 understand these natural hazards [Wu & Wang, 2007]. Slaking crust (the disintegration of

47 ploughed clods) is a key factor that controls runoff and erosion because of its influence on

48 infiltration capacity [Cazenave & Valentin, 1992; Govers et al., 2000; King & Le Bissonnais,

49 1992; Le Bissonnais & Singer, 1992]. Similarly, by conditioning the distribution of rainfall

50 between infiltration, surface retention and runoff [Auzet et al., 2005; Cerdan et al., 2002; Valentin,

51 2005], soil moisture and surface roughness play an important role in risk assessment [Loumagne et

52 al., 1991, 2001; Oudin et al., 2003]. Nevertheless, monitoring and modeling these soil surface

53 characteristics remain difficult because of their substantial variation over space and time [Boiffin

54 et al., 1988; Brown et al., 1990; Zobeck & Onstad, 1987].

55 In this context, satellite imagery is a powerful tool that can provide accurate and repetitive spatial

56 data. Synthetic-aperture radar (SAR) techniques are particularly useful because they make it

57 possible to monitor soil parameters under any weather conditions [Dobson & Ulaby, 1986; Fung,

58 1994; Hallikainen et al., 1985; Ulaby et al., 1986]. For bare agricultural soils, the backscattered

59 radar signal depends strongly on the geometric characteristics (roughness) and dielectric properties

60 (moisture content, soil composition) of the soil. Many studies using data collected by space and

61 airborne SAR scatterometers and model simulations have already shown the potential of radar data

62 to retrieve soil parameters (roughness and moisture) [Baghdadi et al., 2002, 2006, 2007, 2008b;

63 Dobson & Ulaby, 1986; Fung et al., 1992; Holah et al., 2005; Le Hegarat et al., 2002; Oh, 2004;

64 Shi et al., 1997; Srivastava et al., 2003-2009; Ulaby et al., 1978; Zribi et al., 2005; Zribi &

65 Dechambre, 2002].

66   Whatever the SAR configuration, the radar signal follows a logarithmic function with the soil-

67   surface roughness [Fung, 1994; Ulaby et al., 1986]. Ulaby et al. (1978) have shown that the

68   influence of surface roughness decreases with increasing radar frequency. The dynamics of the

69   relationship between the radar signal and roughness parameter are stronger in the L-band than in

70   the C- and X-bands [Baghdadi et al., 2008a; Ulaby et al., 1986] Moreover, SAR data are more

71   sensitive to soil roughness at high incidence angles [Baghdadi et *al.,* 2008a, 2008b; Zribi &

72   Dechambre, 2002].

73   The SAR signal increases with increasing soil moisture for values between 0 and 35-40%

74   [Baghdadi et al., 2007; Holah et al., 2005]. Beyond this threshold, the backscattering coefficient

75   becomes constant and then decreases with increasing soil moisture [Holah et al., 2005]. Several

76   studies in the C-band, with the SAR configuration fixed at a single polarization, have shown that

77   the sensitivity of the radar signal to soil moisture is greater at low and medium incidence angles

78   than at high incidence angles (approximately 0.2 dB/% for HH-20°-37° and approximately 0.1

79   dB/% for HH-39°) [Baghdadi et al., 2006, 2008b; Beaudoin et al., 1990; Srivastava et al., 2003;

80   Zribi & Dechambre, 2002].

81   However, few studies have been conducted in the X-band. The first results based on microwave

82   measurements in the X-band have shown that an incidence angle of 25° is appropriate to observe

83   soil moisture [Singh, 2005]. For the TerraSAR-X sensor, Paris Anguela et al. (2010) have found

84   that the sensitivity of the radar signal to soil moisture is approximately 0.35 dB/% for the HH-25°

85   configuration.

86   The surface area of soil particles in a soil depends on the particle sizes which control the

87   percentage of free and bound water [Srivastava et al., 2009]. Few studies have analyzed the

88   response of the radar signal to soil composition in terms of grain-size distribution (percentages of

89   sand and clay), but several studies have evaluated the effect of salt content on the radar signal.

90   These studies have underlined the influence of salt concentrations on dielectric properties [Aly et

91   al., 2007; Lasne et al., 2008; Shao et al., 2003; Taylor, 1996]. Several studies have recommended

92   high radar wavelengths (L-band) and wet soil conditions for better discrimination between saline

93   and non-saline soil. Under the wettest conditions (soil moisture greater than 30%), the effects of

94   salinity on the C-band are important for sandy soil but do not appear clearly in soils of finer

95   composition due to salt retention by fine particles, such as silt and clay [Aly et al., 2007]. Also,

96   grain-size distribution has an effect on dielectric behavior over the entire frequency range (1.4 to

97   18 GHz) and is most pronounced at frequencies below 5 GHz [Hallikainen et al., 1985]. In the C-

98   band, decreasing soil clay content increases the sensitivity of the radar signal to soil moisture (0.22

99   dB/% for clay soil: 49% clay, 35% silt and 16% sand; 0.33 dB/% for loamy soil: 17% clay, 48%

100   silt and 35% sand) [Ulaby et al., 1978]. Because the distribution of grain sizes controls the amount

101   of free water that interact with the incident microwave, the amount of free water gives significant

102   contribution to SAR backscatter [Srivastava et al., 2006, 2009]. Recent methodology developed to

103   retrieve soil moisture is based on this amount of free water which is controled by the grain size

104   distribution [Srivastava et al., 2009].

105   In the X-band at HH polarization, Prakash et al. (2009) have shown a relationship between the

106   specular scattering coefficient for bistatic scatterometer data and the sand percentage in the soil

107   when surface roughness is less than 1.4 cm. For the TerraSAR-X sensor, Paris Anguela et al.

108   (2010) have also shown (based on one plot and one SAR acquisition at HH-25°) that the SAR

109   signal is 3 dB weaker for a soil composition with more clay (32% clay, 64.5% silt and 3.5% sand)

110   than for a soil with less clay (17% clay, 79% silt and 4% sand).

111   Because soil slaking depends primarily on material properties (moisture, organic-matter content

112   and carbonate content) and decreases infiltration rates, the backscattered radar signal may be

113   sensitive to this soil parameter. Nevertheless, few studies have examined the effect of soil slaking

114   on the radar signal. In the X-band, Stolp & Janse (1986) have carried out a multiple linear

115   regression to relate the backscattering coefficient (HH-15°) to the degree of slaking, the direction

116   of tillage and the incidence angle. Their results are promising and provide good estimates of the

117   degree of slaking (with an accuracy between 78% and 56%).

118   Finally, soil parameters are usually estimated from SAR imagery at plot or watershed scales. Few

119   studies have been conducted at the within-plot scale. In fact, the speckle effects and low resolution

120   (between 10 and 30 m) of the first-generation SAR data (ERS, RADARSAT-1 and ASAR)

121   prevented the analysis of small-scale variations. The high spatial resolution of the TerraSAR-X

122   sensor (1 m) provides access to soil-surface heterogeneities at a finer scale. Baghdadi et al. (2008a)

123   have already mentioned signal variations from TerraSAR-X images within agricultural plots.

124   Quantitative analysis were not conducted, but only observations were given from photo-

125   interpretation of SAR images. Paris Anguela et al. (2010) have made a preliminary diagnostic with

126   an analysis from only one bare agricultural plot and in using only one TerraSAR image. In the

127   present work we consolidated and completed these previous investigations in using large database

128   of in situ measurements (soil composition, soil moisture and observations concerning the presence

129   or the absence of crust) and TerraSAR-X images at different radar incidence angle.

130   The main objective of this study is to analyze the potential of the TerraSAR-X radar sensor to

131   characterize soil-surface parameters at the plot and within-plot scales. The effects of soil moisture,

132   roughness, soil composition and slaking crust on the TerraSAR-X backscattering coefficient are

133   analyzed only over agricultural plots.

134

2.   MATERIAL AND METHODS

2.1.   STUDY SITE

137   The study site is the Orgeval watershed (104 km²), which is located to the east of Paris (France;

138   48°51'N 3°07'E; Figure 1). The site has been managed since 1962 as an experimental basin for

139   hydrological research by the Agricultural and Environmental Engineering Research Center

140 (CEMAGREF) research institute. The Orgeval watershed is mostly composed of agricultural plots

141 intended for growing wheat and maize. It is flat and composed of loamy soils with average

142 percentages of 17% clay, 78% silt, and 5% sand. This soil structure promotes crust development,

143 which increases soil sealing and causes runoff [Boiffin et al., 1990; Eimberck, 1990].

144

145 **2.2.   SATELLITE DATA**

146 **2.2.1. SAR data**:

147 Fourteen TerraSAR-X images (X-band) were acquired in 2009 and 2010 in Spotlight mode (pixel

148 spacing ~1 m) with HH polarization and incidence angles of 25° and 50°. The incidence angles of

149 each TerraSAR image are summarized in Table 1.

150 Radiometric calibration of the MGD (Multi Look Ground Range Detected) TerraSAR images was

151 carried out using the following equation [Fritz, 2007]:

$$\sigma° = (Ks \cdot DN^2 - NEBN) \cdot \sin(\theta) \tag{1}$$

152 This equation transforms the digital number of each pixel DN (amplitude of the backscattered

153 signal) into a backscattering coefficient (σ^o) corrected for sensor noise (NEBN) on a linear scale.

154 This calibration takes into account the radar incidence angle (θ) and the calibration constant (Ks)

155 provided in the image data. The backscattering coefficients are then calculated in decibels by the

156 following formula:

$$\sigma^o_{dB} = 10 \cdot \log_{10}(\sigma°) \tag{2}$$

157 This radiometric calibration makes it possible to perform multi-temporal analysis of the different

158 images. All of the images were then co-registered using aerial orthophotos (50-cm spatial

159 resolution) with a root mean square error of the control points of approximately one pixel (i.e., 1

160 m). This co-registration error was overcome by removing the boundary pixels (two pixels wide)

161 from each training plot relative to the limits defined by the GPS control points.

162

163 **2.2.2. Optical data**:

164 One optical IKONOS image was acquired on March 14, 2009 in multispectral mode (pixel spacing

165 ~ 4 m). The IKONOS image was calibrated for TOA (top of atmosphere) reflectance and co-

166 registered using aerial orthophotos with a root mean square error of the control points of

167 approximately one pixel (i.e., 4 m).

168

169 **2.3.   EXPERIMENTAL MEASUREMENTS**

170 Simultaneously to the TerraSAR-X acquisitions, ground measurements were performed in thirteen

171 bare training plots in 2009 and 2010 (± three hours around the satellite overpass time) (Figure 2).

172 All training plots were flat (slope < 1%). Four soil-surface parameters were observed or measured:

173 moisture content (at the 0-5-cm depth), surface roughness, soil composition, and slaking crust.

174 Meteorological data (precipitation and temperature) were also obtained from five meteorological

175 stations installed in the basin. Each station is less than 5 km from the center of each plot. Figure 3

176 shows the mean values of meteorological data recorded in 2009 (a) and 2010 (b) at the five

177 stations.

178

179 **2.3.1. Soil roughness ($Hrms$):**

180 Measurements of soil roughness were carried out in all of the training plots using 1-m-long needle

181 profilometers with 2-cm sampling intervals. Ten roughness profiles along and across the direction

182 of tillage (five parallel and five perpendicular) were established in each training plot. Two

183 parameters can be calculated from these measurements: the average root mean square surface

184 height (*Hrms*) and the correlation length (*l*) [Ulaby et al., 1986]. The *Hrms* values of the plots

185 obtained during the two field surveys (March to May 2009 and March 2010) varied between 0.4

186 and 3.9 cm. The lower values (0.4 to 1.5 cm) corresponded to sown plots, whereas the higher

187 values (above 1.5 cm) corresponded to fallow and recently ploughed plots. The correlation length

188 (*L*) varies from 2.3 cm in sown fields to 9.3 cm in ploughed fields. As shown in Figure 4, the

189 relationship between the *Hrms* and the correlation length can be modeled by a linear regression

190 [Davidson et al. 2003, Baghdadi et al. 2008a]. Nevertheless, inverting the two parameters *Hrms*

191 and *L* separately in the inversion of radar measurements seems to be a difficult task because our

192 TerraSAR images contain a single band per pixel (one polarization and one incidence angle).

193 The error on the roughness computation is influenced mainly by the roughness profiles length, the

194 number of profiles, and the horizontal resolution (sampling interval) of profiles.

195 According to Oh and Kay (1998), the roughness profiles length should be at least 40*L* and 200*L*

196 (where *L* is the correlation length) in order to obtain the *Hrms* and the correlation length with a

197 precision of 10%. Lievens et al. (2009) and Callens et al. (2006) have demonstrated that shorter

198 profiles result in lower *Hrms* and correlation length. A significant underestimation of roughness

199 parameters is observed for short profiles and large correlation length. The number of averaged

200 profiles that is required to obtain a standard deviation on *Hrms* and *L* less than 10% is dependent

201 of profile length. Lievens et al. (2009) demonstrated that less than 10 averaged profiles are

202 required for 1 m profile to obtain a standard deviation of *Hrms* lower than 10%, whereas the same

203 accuracy (better than 10%) for correlation length only becomes feasible for at least 15 averaged

204 profiles. The precision on the correlation length measurements should be about 15 to 20% for the

205 range of correlation length measured within our bare agricultural fields, with 1m profile and 10

206 average profiles (higher standard deviation for large correlation length). The precision associated

207 with the measurements of *Hrms* and *L*, were also dependent on the horizontal spacing between

208 height points (Δx). Oh and Kay (1998) suggested that the surface should be sampled at a spacing

209   no longer than 0.2L and no more than 0.5L for the same precision of about 5% on the correlation

210   length and the *Hrms* surface height, respectively. For our range of correlation length, the accuracy

211   of roughness parameters with a spacing of 2 cm should be better than ± 10% for *Hrms* and

212   between ± 10% and ± 20% for large and small correlation lengths, respectively. According to

213   Lievens et al. (2009), an increase in horizontal spacing causes a decrease in *Hrms* and an increase

214   in correlation length, which are more pronounced for surfaces with small correlation length.

215   Moreover, the standard deviation of roughness parameters with a spacing of 1.5 cm is better than

216   ±5% for *Hrms* and better than ±15% for correlation length.

217   Also, only the relationship between the *Hrms* surface height and the radar signal was used in this

218   study; ten 1-m-long profiles are not sufficient to estimate L parameter with accuracy lower than

219   15% [Oh & Kay, 1998].

220   Finally, most of our training plots don't have marked row directions because they correspond to

221   old winter ploughed without row direction (isotropic surface).

222

2.3.2. Soil moisture (*mv*):

224   In most studies of microwave measurements carried out over bare soils, experimental relationship

225   between soil moisture and backscattering coefficient are provided by mean volumetric water

226   contents measured to a soil depth, generally 0-5 cm. At X-band, no experimental measurements

227   were conducted in field condition and the low penetration of this radar wavelength is only based

228   on theoretical study. So, the penetration depth of the X-band is not yet known.

229   In this study, between fifteen and twenty-eight gravimetric soil-moisture samples (depth: 0-5 cm)

230   were collected per day for each training plot. The location of each gravimetric measurement was

231   recorded using a GPS device.

232   All gravimetric measurements were converted into volumetric moisture (mv) based on bulk

233   density. Five bulk-density measurements were made for each training plot using 9-cm-long

234   cylindrical samples with volumes of 500 cm^{-3}. Bulk-density values varied between 0.9 and 1.4

235   g.cm^{-3}. The soil moisture of each plot (or part of a plot) was assumed to be equal to the mean value

236   estimated from the samples collected in that plot (or part of a plot). The two field surveys in 2009

237   and 2010 covered a large range of soil moisture, between 12.6% and 39.8% (see Table 1). The

238   standard deviation of soil moisture measurements varied between 0.6% and 2.75%per each

239   training plot (or part of a plot).

240

241   **2.3.3. Soil composition**:

242   Soil composition was analyzed only in the training plots studied in 2009. For each training plot,

243   ten soil samples were analyzed for their percentages of clay, sand and silt. The analysis showed

244   that the surface soils within the training plots could be classified into two categories of loam:

245   -   soil I: clay = 24% ± 1.9%; silt = 71% ± 1.7%; sand = 5% ± 1.5%.

246   -   soil II: clay = 16% ± 0.9%; silt = 78% ± 2%; sand = 6% ± 1.3%.

247   The major differences between these two soils corresponded to small variations in clay and silt

248   content (clay = 8%, silt = 7%). The largest difference in clay content between soil I and soil II was

249   found in plot D (~10%), and the smallest value was found in plot G (~3%). The differences in sand

250   content were very small (mean ~1%).

251

252   **2.3.4. Slaking crust:**

253   The structure of bare soils can be modified by the energy of impact of raindrops, and a slaking

254   crust can be formed on the soil surface. A slaking crust decreases the infiltrability of the soil,

255   favoring runoff. This phenomenon is commonly observed on loamy soils and is dependent on soil

256   composition (clay and silt content, organic matter and carbonate content).

257   The presence or absence of slaking crust on the soil surface was noted during the 2009 field

258   survey. Slaking crust blocks the porosity of the soil surface, creating a layer of compacted soil that

259   is often visible to the naked eye. The stagnation of water and the presence of a thin, continuous

260   and consistent surface layer (crust) indicate the spatial extent of the slaking crust.

261   In March 2009, we observed slaking crust with a thickness of approximately 1 cm on soil II

262   (16% ± 0.9% clay, 78% ± 2% silt and 6% ± 1.3% sand). In April and May 2009, no slaking crusts

263   were observed within the training plots due to tillage operations that had removed the soil crusts

264   and increased the porosity of the topsoil.

265

266   **3. RESULTS**

267   **3.1. TERRASAR-X SIGNAL AND SOIL-SURFACE ROUGHNESS**

268   For bare soils, surface roughness plays an important role in the amount of energy returned to the

269   radar instrument. The sensitivity of the TerraSAR-X signal ($\sigma°$) in HH polarization to surface

270   roughness ($Hrms$) at the plot scale was analyzed for both incidence angles (25° and 50°). The

271   database was classified into three soil-moisture groups: $10\% < m_v < 15\%$ (low), $15\% < m_v < 25\%$

272   (medium) and $25\% < m_v < 40\%$ (high). For each incidence angle and soil-moisture group, the

273   relationship between $\sigma°$ and $Hrms$ was analyzed.

274   For high soil moisture, $\sigma°$ could be modeled by a logarithmic function according to $Hrms$ for either

275   incidence angle (Figures 4a and 4b), and $\sigma°$ was more sensitive to surface roughness at a high

276   incidence angle (50°) than at a low incidence angle (25°). The mean difference between the $\sigma°$

277   values of the smoothest ($Hrms = 0.7$ cm) and roughest areas ($Hrms = 3$ cm) reached a maximum of

278   1.9 dB at 25° (Figure 5a) and approximately 3.5 dB at 50° (Figure 5b). Similar dynamics of the

279 TerraSAR-X signal and surface roughness have been observed by Baghdadi et *al.* (2008a).

280 Moreover, at an incidence angle of 25°, the backscattering coefficient quickly reaches its

281 maximum level for an *Hrms* of approximately 0.8 cm (Figure 5a). Beyond this threshold, the

282 backscattering coefficient becomes constant regardless of the roughness. Roughness values of less

283 than 0.8 cm are rare in agricultural areas. Therefore, for agricultural applications, soil-roughness

284 mapping is not feasible using X-band SAR data at a low incidence angle.

285 For medium soil moisture, the backscattering coefficient was almost constant for *Hrms* surface

286 heights between 1.1 and 2.7 cm at either incidence angle (Figures 4a and 4b).

287 The lack of roughness data for low soil-moisture conditions made it possible to perform only

288 partial observations for the 50° incidence angle. As observed for medium soil moisture, σ° values

289 for low soil moisture seem to be independent of surface roughness for *Hrms* surface heights

290 between 1.1 and 2.7 cm (Figure 5b).

291 The backscattering coefficients of soils with the same roughness but different soil-moisture levels

292 (medium and high) were also compared. At a 25° incidence angle and for *Hrms* values between

293 1.1 and 2.7 cm, the backscattering coefficient of a soil with medium moisture content was

294 approximately 4.0 dB lower than that of the same soil with high moisture content (Figure 5a). This

295 difference of 4.0 dB was larger than that observed between smooth (*Hrms* ~ 0.4 cm) and rough

296 (*Hrms* ~ 3 cm) soils (1.9 dB). At a 50° incidence angle and for *Hrms* surface heights between 0.8

297 and 2.7 cm, the backscattering coefficient of a soil with medium moisture content was

298 approximately 1.5-5 dB lower than that of the same soil with high moisture content (Figure 5b).

299 The difference in the backscattering coefficient between soils with different levels of moisture was

300 smaller than the dynamics of the backscattering coefficient with changes in roughness at high soil

301 moisture (3 dB for *Hrms* values between 0.8 and 2.7 cm, Figure 5b) for the smoothest areas and

302 larger for the roughest areas. The lack of roughness data with low moisture content made it

303 possible to perform only partial observations. At a 50° incidence angle and for *Hrms* values

304   between 1.2 and 2.9 cm, the backscattering coefficient for low soil moisture was lower by

305   approximately 4-6 dB than that of soils with high soil moisture (Figure 5b). This difference was

306   larger than the difference in backscattering coefficient between soils with different levels of

307   roughness at high soil moisture (2.1 dB for *Hrms* between 1.2 cm and 2.9 cm, Figure 5b).

308   In conclusion for agricultural bare plots, the effects of soil roughness on the TerraSAR-X signal

309   are small and function of the moisture content. Consequently, the backscattering coefficient σ°

310   (dB) in the X-band cannot be expressed as the sum of one function dependent on soil moisture and

311   another dependent on *Hrms* surface height, as is commonly assumed for the L- and C-bands

312   [Baghdadi et al., 2006; Zribi & Deschambre, 2002].

313

314   **3.2. TERRASAR-X SIGNAL AND SOIL MOISTURE CONTENT**

315   The high spatial resolution of the TerraSAR data (1 m) made it possible to analyze the radar signal

316   according to soil moisture at the plot and within-plot scales. The mean backscattering coefficient

317   was estimated for each training plot according to the scale of interest and plotted as a function of

318   in situ soil-moisture measurements regardless of roughness. Figure 6 illustrates the dynamics of

319   the radar backscattering coefficient versus soil moisture for HH polarization at low (25°) and high

320   (50°) incidence angles. Overall, the scattering behavior of the soil increased with soil moisture.

321   The wide range of soil-moisture measurements (13-40%) made it possible to establish linear

322   relationships between the radar signal and the soil moisture for each incidence angle. The

323   sensitivity of the radar signal to soil moisture was 0.411 dB/% for the TerraSAR-X data at 25°

324   (Figure 6a). Paris Anguela et al. (2010) have observed a sensitivity of the same order using a

325   single TerraSAR-X image and simulated data from the IEM model (X-HH-26°: 0.35 dB/%). For

326   the high incidence angle (50°), the sensitivity of the TerraSAR-X signal to soil moisture decreased

327   to 0.323 dB/% (Figure 6b). This analysis demonstrates that the SAR signal in the X-band is

328   slightly more sensitive to soil moisture at a low incidence angle (25°), but soil-moisture mapping

329   can be carried out with either low or high incidence angles (because both showed high

330   sensitivities). This decreasing radar sensitivity with increasing incidence angle is consistent with

331   other studies performed using C-band SAR data. Indeed, several studies using C-band data (ERS,

332   RADARSAT, ASAR) have shown higher sensitivities between the radar signal and soil moisture

333   for low incidence angles (0.2-0.3 dB/%) than for high incidence angles (0.1 dB/%) [Baghdadi et

334   al., 2008a; Le Hégarat et al., 2002; Quesney et al., 2000; Srivastava et al., 2003]. Finally, the

335   sensitivity of the radar signal to soil moisture appears to be higher in the X-band than in the C-

336   band, regardless of the incidence angle. Theoretical surface backscattering models show

337   approximately the same sensitivity between radar signal and soil moisture for these two radar

338   wavelengths (Fung, 1994). The increasing in the sensitivity of radar signal to soil moisture at X-

339   band could be due particularly to volume scattering effect. First, radar signal increases with soil

340   moisture for C- and X-bands. In the other hand, the volume scattering term is certainly higher at C-

341   band than at X-band for low and medium moistures due to more important penetration of waves.

342   This means that at C-band, the dynamic of radar signal with soil moisture variation could be lower

343   at C-band because of this scattering term added for low and medium soil moistures. This decrease

344   in radar dynamic induces a decreasing of sensitivity at C-band.

345

346   **3.3. TERRASAR-X SIGNAL AND SOIL COMPOSITION**

347   The sensitivity of the TerraSAR-X signal to soil composition was studied using images acquired in

348   2009 because the soil-composition analysis focused on the training plots measured in 2009.

349   Heterogeneities within plots were observed in the TerraSAR-X images only on March 17 and 18,

350   2009 (Figures 2 and 7). These variations within the training plots were also observed in the

351   IKONOS image (Figure 7j).

352   To investigate these differences, soil samples were taken in each training plot to determine the

353   particle-size distribution within plots. According to the soil-composition analysis, the zones with

354 low radar-signal values (darker zones) were more clayey (soil I: 24% clay, 71% silt and 5% sand)

355 than the zones with high radar-signal values (brightest zones; soil II: 16% clay, 78% silt and 6%

356 sand). Also, the variations in the TerraSAR-X signal within plots were spatially correlated with the

357 variations in soil composition on the two acquisition dates (March 17 and 18).

358 The mean differences in σ° between soil-II zones and soil-I zones had the same order of magnitude

359 for the HH-25° (March 17: 2.6 dB) and HH-50° (March 18: 2.3 dB) configurations. Indeed, these

360 two acquisitions occurred within an interval of less of 24 hours (ensuring the same surface

361 conditions). Thus, according to these observations, the TerraSAR-X data allow to map limits of

362 our two soils within the plots regardless of the incidence angle.

363 Simulations using the IEM radar-backscattering model [Fung, 1994] were also carried out for the

364 two soil compositions (I and II). The surface-roughness (*Hrms*, *l*) and soil moisture *(mv)* values

365 measured during the field survey were used to run the simulations. In the IEM model, the

366 Hallikainen equations [Hallikainen et al., 1985] are used to calculate the dielectric constant

367 according to the percentages of sand and clay. Our results showed that the X-band data did not

368 discriminate the two soil categories (the variations between these soil categories were less than 1

369 dB in the X-band). These results were expected because the difference in soil composition between

370 soil categories II and I was small. Indeed, the two soil compositions measured within the plots had

371 a maximum mean difference in clay content of approximately 10% (training plot D). Several

372 studies in the C- and L-bands have shown that the radar signal is directly dependent on the amount

373 of sand and clay, but only for soil compositions that are very different (differences in clay content

374 of more than 30%) [Dobson & Ulaby, 1981; Schmugge et al., 1976; Ulaby et al., 1978].

375 Similarly, the mean differences in sand content between the two soil categories did not exceed 1%.

376 Prakash et al. (2009) has shown that the specular-scattering coefficient of X-band bistatic

377 scatterometer data at HH polarization is strongly dependent on the percentage of sand in the soil

378 when the surface is smooth. The change in the specular-scattering response with variations in soil

16

379   composition is difficult to observe when the soil is rough (*Hrms* > 1.4 cm). On March 2009, the

380   smoothest training plots had a roughness of approximately 1.9 cm. Therefore, changes in

381   scattering with changes in soil composition within our rough plots were not clear in the TerraSAR

382   data.

383   Thus, the TerraSAR-X signal was not directly sensitive to the soil composition in our training

384   plots. Nevertheless, the spatial variation in the TerraSAR signal at the within-plot scale was

385   correlated with the spatial distribution of soil composition in some TerraSAR-X acquisitions.

386   Therefore, soil composition should affect other soil parameters that directly influence the

387   TerraSAR-X signal.

388

389   **3.4. TERRASAR-X SIGNAL AND SOIL CRUST**

390   During the field survey in March 2009, slaking crust was observed on soil II and not on soil I. We

391   studied the effect of the soil-II crust on the radar signal for seven training plots of 2009. Because

392   soil crusts modify the water-retention properties and infiltration rates of the soil [Augeard, 2006;

393   Musy & Soutter, 1991], the differences in soil moisture between soil II and soil I ($mv_{soil\ II}$ - $mv_{soil\ I}$)

394   were compared to the differences in the TerraSAR signal ($\sigma°_{soil\ II}$ - $\sigma°_{soil\ I}$). The acquisitions on

395   March 17 and 18, 2009 differed from the other 2009 acquisitions by their greater variation in

396   signal and soil moisture within the training plots. The mean difference in signal calculated from

397   the March 17 and March 18 images between the soil-II and soil-I zones was approximately +2.5

398   dB (Table 3) for a mean difference in moisture content of approximately +4.5% (2.9-7.2%,

399   depending on the training plot) (Table 2). The difference in soil moisture between soils I and II can

400   be explained by the difference in the soil-surface structure (i.e., the presence or absence of slaking

401   crust). During the winter dry period (March 11 to March 22, Figure 3), soil I dries faster than soil

402   II. In soil II, evaporation is limited by the crust, and the moisture content is retained longer than in

403   soil I. Thus, the moisture-content values of soil I were lower than those of soil II. Because the

404 TerraSAR signal is highly sensitive to soil moisture (section 3.2), the variations in moisture

405 content between the two soils generated differences in the backscattered signal.

406 On March 25 and 26, the mean difference in signal between soil-II and soil-I zones was less than 1

407 dB (Table 3) for an average difference in moisture content of less than 1% (Table 2). Thus, no

408 variation in either soil moisture or TerraSAR-X signal was observed within the plots on these

409 dates. After rainy events (2.7 mm on March 23 and 4.7 mm only three hours before the March 25

410 acquisition; Figure 3), the moisture content of soil I increased strongly (by approximately +4.5%)

411 because soil I absorbed both precipitation and streaming water coming from soil II. The moisture

412 content of soil II increased slightly (by approximately 1%) because the soil crust prevented water

413 infiltration and favored hydric inertia. On March 17 and 18, soil II had greater moisture content

414 than soil I. Because the moisture content of soil I increased and the moisture content of soil II

415 stayed constant, the difference in moisture content between the two soils disappeared. For the

416 other acquisition dates between April 8 and May 11, 2009, tillage had destroyed the soil crust and

417 increased the porosity of soil II. Without crust, the compositions of the two soils were too similar

418 to generate a difference in moisture content between soil I and soil II (< 1%), and no differences in

419 signal were observed between the two soils.

420 Thus, variations in the TerraSAR-X signal within plots were correlated with differences in the

421 soil-surface structure between the two soils. The slaking crust on soil II generated differences in

422 moisture content between soil I and soil II under certain conditions. For a single training plot

423 located within the same study area, Paris Anguela et al. (2010) have shown that a soil with a

424 smaller percentage of clay (soil B: 17% clay, 79% silt and 4% sand) had a TerraSAR signal (HH-

425 25°) 3 dB stronger than that of a more clayey soil (soil A: 32% clay, 64.5% silt and 3.5% sand).

426 The driest upper millimeters of soil B and the low X-band penetration at high moisture content

427 [Nolan & Fatland, 2003] were used to explain the difference in signal between soil B and soil A.

428

429 **4. CONCLUSIONS**

430 This study analyzes the potential of high-spatial-resolution data from the TerraSAR-X sensor to

431 monitor the soil-surface characteristics of bare agricultural soils (roughness, moisture, composition

432 and structure) at plot and within-plot scales. The backscattering coefficients obtained from multi-

433 temporal SAR acquisitions at HH polarization and two incidence angles (25° and 50°) were

434 compared to ground observations and measurements. Our results are promising for retrieving soil

435 moisture information from TerraSAR-X data and for monitoring the dynamics of slaking crust

436 hydric states within plots. The results are summarized below.

437 ➤ For high soil moisture ($25 < m_v < 40\%$), the sensitivity of the TerraSAR-X backscattering

438   coefficient to soil roughness is slightly higher at a 50° incidence angle (3.5 dB) than at a

439   25° incidence angle (1.9 dB). Moreover, for either incidence angle, the variation in the

440   radar signal with surface roughness is smaller for soils with moisture contents between

441   15% and 25% than for soils with moisture contents over 25%. The sensitivity of the

442   TerraSAR signal at 25° to soil roughness for areas with high moisture content (25% < mv

443   < 40%) is lower than the difference in signal between two areas with different moisture

444   contents (15% < mv < 25% and 25% < mv < 40%). At 50°, the change in σ° with surface

445   roughness for high soil moisture is larger than the variation in the signal between two

446   smooth soils (*Hrms* ~ 0.8 cm) with different soil moisture levels (15% < mv <25% and

447   25% < mv < 40%) and is slightly smaller in the case of rough areas (*Hrms* ~ 2.7 cm).

448   Therefore, in the X-band, a high incidence angle (50°) is the optimal configuration for soil-

449   roughness monitoring in agricultural areas (bare soils).

450 ➤ The sensitivity of the TerraSAR-X signal to soil moisture is greater at a low incidence

451   angle than at a high incidence angle (25°: 0.411 dB/%; 50°: 0.323 dB/%). Thus, an increase

452   in moisture content of approximately 5% generates an increase in the backscattered signal

453   of approximately 2.0 dB at a 25° incidence angle and 1.6 dB at a 50° incidence angle.

454 ➤ The X-band SAR signal is not sensitive to slight differences in soil composition in bare

455 agricultural fields (the maximum differences in our plots were 10% in clay and 1% in

456 sand). No direct influence of soil composition on the radar signal was observed.

457 Nevertheless, two TerraSAR-X acquisitions have shown signal variations within reference

458 plots in the Orgeval study site that are spatially correlated with differences in soil

459 composition at both high (50°) and low (25°) incidence angles (March 17 and 18, 2009).

460 No TerraSAR-X signal variations were observed without crust or when there were no

461 contrast of soil moisture between the soil crusted (II) and not crusted (I). So, when

462 variations of composition engender variations of soil moisture (due to variations of soil

463 structure and meteorological conditions), the spatial extent of soil composition can be

464 observed within plots on TerraSAR-X signal.

465 ➤ Variations in the TerraSAR-X signal within reference plots are correlated with the hydric

466 evolution of soil crust. Soil with slaking crust (soil II) has a greater hydric inertia than soil

467 without crust (soil I). Consequently, following rainfall or dry events, soil moisture in the

468 upper centimeters may differ between the two soil structures, resulting in variations in the

469 TerraSAR-X signal within the field. Thus, it is sometimes possible to track surface

470 degradation due to the slaking process using the TerraSAR-X sensor.

471 Because of the low sensitivity to surface roughness and the high sensitivity to soil moisture, the

472 use of TerraSAR-X data at HH polarization with a single incidence angle is a promising method

473 for estimating soil parameters. Further studies are needed to analyze the complementary

474 polarizations and incidence angles. Similarly, the synergy between the X-band (TerraSAR-X) and

475 other SAR wavelengths (PALSAR/ALOS, RADARSAT-2, ASAR/ENVISAT) should be

476 examined.

477

478 **Acknowledgments**

484

485   **References**

486   **Aly, Z., Bonn, F. J., Magagi, R. (2007)**. Analysis of the backscattering coefficient of salt-affected

487   soils using modeling and radarsat-1 SAR data. *IEEE Transactions on Geoscience and Remote*

488   *Sensing, vol. 45, n° 2: 332 – 341*

489   **Augeard, B. (2006).** Mécanismes de genèse du ruissellement sur sol agricole drainé sensible à la

490   battance. Etudes expérimentales et modélisation. *Doctorat Sciences de l'eau, Unité de Recherche*

491   *Hydrosystèmes et Bioprocédés, ENGREF 06ENGR0010, 236 p.*

492   **Auzet, A.V., Kirkby, M.J., Van Dijk, P. (2005).** Surface characterisation for soil erosion

493   forecasting. *Catena, vol. 62, n° 2–3: 77–78.*

494   **Baghdadi, N., Gaultier, S., King, C. (2002).** Retrieving surface roughness and soil moisture from

495   SAR data using neural network. *Canadian Journal of Remote Sensing vol. 28, n° 5: 701–711.*

496   **Baghdadi, N., Holah, N., Zribi, M., (2006).** Soil moisture estimation using multi-incidence and

497   multi-polarization ASAR SAR data. *International Journal of Remote Sensing, vol. 27, n° 10:*

498   *1907–1920.*

499   **Baghdadi, N., Aubert, M., Cerdan, O., Franchistéguy, L., Viel, C., Martin, E., et al. (2007).**

500   Operational mapping of soil moisture using synthetic aperture radar data*: application to Touch*

501   basin (France). *Sensors Journal, vol. 7: 2458−2483.*

502 **Baghdadi, N., Zribi, M., Loumagne, C., Ansart, P., & Paris Anguela, T. (2008a).** Analysis of

503 TerraSAR-X data and their sensitivity to soil surface parameters over bare agricultural fields.

504 *Remote sensing of Environnement, vol. 112, n° 12: 4370-4379.*

505 **Baghdadi, N., Cerdan, O., Zribi, M., Auzet, V., Darboux, F., El Hajj, M., et al. (2008b).**

506 Operational performance of current synthetic aperture radar sensors in mapping soil surface

507 characteristics*:* application to hydrological and erosion modelling. *Hydrological Processes, vol.*

508 *22, n° 1: 9−20.*

509 **Beaudoin, A., Gwy, Q.H.J., Le Toan, T. (1990).** SAR observation and modelling of the C-band

510 backscatter variability due to multi-scale geometry and soil moisture. *IEEE Transactions on*

511 *Geoscience & Remote Sensing, vol. 28:* 886-894.

512 **Boiffin, J., Papy F., & Eimberck, M. (1988).** Influence des systèmes de culture sur les risques

513 d'érosion par ruissellement concentré : Analyse des conditions de déclenchement de l'érosion.

514 *Agronomie, vol. 8: 663-673.*

515 **Callens, M., Verhoest, N., Davidson, M. (2006).** ParametrizationCondition for precise

516 measurement of soil surface roughness. *IEEE Transactions on Geoscience and Remote Sensing,*

517 *vol. 36, n° 2: 691 – 695.*

518 **Cerdan, O., Poesen, J., Govers, G., Saby, N., Le Bissonnais, Y., Gobin, A., Vacca, A.,**

519 **Quinton, J., Auerswald, K., Klik, A., Kwaad, F.J.P.M., Roxo, M.J. (2006).** Sheet and rill

520 erosion rates in Europe. *In soil Erosion in Europe, Boardman J., Poesen J (eds), chap. 38. Wiley :*

521 *Chichester, UK: 501−513.*

522 **Davidson, M., Mattia, F., Satalino, G., Verhoest, N., Le Toan, T., Borgeaud, M., Louis, J.,**

523 **Attema, E. (2003).** Joint statistical properties of RMS height and correlation length derived from

524 multisite 1-m roughness measurements. *IEEE Transactions on Geosciences and Remote Sensing,*

525 *vol. 41: 1651-1658.*

526 **Dobson, M.C., & Ulaby, F.T. (1981).** Microwave backscatter dependence on surface roughness,

527 soil moisture and soil texture: Part III- soil tension. *IEEE Transactions on Geosciences and*

528 *Remote Sensing, vol. 19: 51-61.*

529 **Dobson, M.C., & Ulaby, F.T. (1986).** Active microwave soil moisture research. *IEEE*

530 *Transactions on Geoscience and Remote Sensing, vol. GE-24, n° 1: 23-36.*

531 **Eimberck, M. (1990).** Facteurs d'érodibilité des sols limoneux: réflexions à partir du Pays de

532 Caux. Cah. (In French.). *ORSTOM, série Pédologique, vol. XXV, n° 1-2: 81–94.*

533 **Fung, A.K., & Chen, K.S. (1992).** Dependence of the surface backscattering coefficients on

534 roughness, frequency and polarization states. *International Journal of Remote Sensing, vol. 13:*

535 *1663-1680.*

536 **Fung, A,K. (1994)**. Microwave Scattering and Emission Models and their Applications. *Artech*

537 *House, Norwood, Massachussetts : 573 p.*

538 **Fritz, T. (2007).** TerraSAR-X Level 1b Product Format Specification", *TX-GS-DD-3307, n° 1.3.*

539 **Govers, G., Takken, I., Helming, K. (2000).** Soil roughness and overland flow, *Agronomie, vol.*

540 *20: 131-146.*

541 **Hallikaïnen, M., Ulaby, F., Dobson, F., El Rayes, M., & Wu, L. (1985).** Microwave dielectric

542 behavior of wet soil. Part I : Empirical models and experimental observations, *IEEE Transactions*

543 *on Geoscience and Remote Sensing, vol. 23: 25-34.*

544 **Holah, N., Baghdadi, N., Zribi, M., Bruand, A., & King, C. (2005).** Potential of

545 ASAR/ENVISAT for the characterization of soil surface parameters over bare agricultural fields.

546 *Remote Sensing of Environnement, vol. 96, n° 1: 78-86.*

547 **King, D., & Le Bissonnais, Y. (1992)**. Rôle des sols et des pratiques culturelles dans l'infiltration

548 et l'écoulement des eaux . Exemple du ruissellement et de l'érosion sur les plateaux limoneux du

549 nord de l'Europe. *C. R. Acad. FR., vol. 78, n° 6: 91-105.*

550 **Lasne, Y., Paillou, Ph., Ruffié, G., Serradilla, C., Demontoux, F. (2008).** Effect of salinity on

551 the dielectric properties of geological materials: implication for soil moisture detection by means

552 of remote sensing. *IEEE Transactions on Geoscience and Remote Sensing, vol. 46, n° 6: 1674-*

553 *1688.*

554 **Le Bissonnais, Y., & Singer, M.J. (1992).** Crusting, Runoff and erosion Response to soil Water

555 Content and Successive Rainfalls. *Soil Science Society American Journal, vol. 56: 1898-1903.*

556   **Le Hégarat Mascle, S., Zribi, M., Alem, F., Weisse, A., & Loumagne, C. (2002).** soil moisture

557 estimation from ERS/SAR data : toward an operational methodology. *IEEE Transactions on*

558 *Geoscience and Remote Sensing, vol. 40, n° 12: 2647-2658.*

559 **Lievens, H., Vernieuwe, H., Alvarez-Mozos, J., De Baets, B., Verhoest, N., (2009).** Error in

560 radar-derived soil moisture due to roughness parameterization: an analysis based on synthetical

561 surface profiles. *Sensors Journal, vol. 9: 1067−1093.*

562 **Loumagne, C., Michel, C., Normand, M. (1991).** Soil water conditions and forecasting rain

563 water runoff. *Journal of Hydrology, vol. 123: 1-17.*

564 **Loumagne, C., Weisse, A., Normand, M., Riffard, M., Quesney, A.,Le Hegarat-Mascle, S.,**

565 **Alem, F.** *(2001).* Integration of remote sensing data into hydrological models for flood

566 forecasting. *Remote Sensing and Hydrology 2000, IASH Red Book Pub., n°267, edited by*

567 *Brubaker, Ritchie, Rango: 592-594.*

568 **Musy, A., et Soutter, M. (1991).** Physique du sol. *Presses Polytechniques et Universitaires*

569 *Romandes, Lausanne, Suisse, 335p.*

570 **Nolan, M., & Fatland, D.R. (2003).**Penetration Depth as a DInSAR Observable and Proxy for

571 soil Moisture. *IEEE Transactions on Geoscience and Remote Sensing, vol. 41, n° 3:532-537.*

572 **Oh, Y., & Kay, Y.(1998).** Condition for precise measurement of soil surface roughness. *IEEE*

573 *Transactions on Geoscience and Remote Sensing, vol. 36, n° 2: 691 − 695.*

574   **Oh, Y. (2004).** Quantitative retrieval of soil moisture content and surface roughness from

575   multipolarized radar observations of bare soil surfaces. *IEEE Transactions on Geoscience and*

576   *Remote Sensing, vol. 42, n° 3: 596 – 601.*

577   **Oudin, L., Weisse, A., Loumagne, C., Le Hegarat-Mascle, S. (2003).** Assimilation of soil

578   moisture into Hydrological models for flood forecasting a variational approach. *Canadian Journal*

579   *of Remote sensing, vol. 29, n° 6: 679-686.*

580   **Paris Anguela, T., Zribi, M., Baghdadi, N., Loumagne, C. (2010).** Analysis of local variation of

581   soil surface parameters with TerraSAR-X radar data over bare agricultural fields. *IEEE*

582   *Transactions on Geoscience and Remote Sensing vol. 48, n° 2: 874–881.*

583   **Prakash, R., Singh, D., Pathak, N.P. (2009).** Microwave specular scattering response of soil

584   texture at X-band. *Advances in Space Research, vol. 44, n° 7: 801–814.*

585   **Quesney, A., Le Hegarat-Mascle, S., Taconet, O., Vidal-Madjar, D., Wingneron, J.P.,**

586   **Loumagne, C., & Normand, M. (2000).** Estimation of watershed soil moisture index from

587   ERS/SAR data. *Remote sensing of environment, vol. 72, n° 3: 290-303.*

588   **Schmugge, T., Wilheit, T., Webster, W., & Gloerson, P. (1976).** Remote sensing of soil

589   moisture with microwave radiometers-II. *NASA Goddard Space Flight Center, Greenbelt, MD,*

590   *20771. NASA Technical Note TN-D-8321.*

591   **Shao, Y., Hu Q., Guo, H., Lu, Y., Dong, Q., Han, C. (2003).** Effect of dielectric properties of

592   moist salinized soils on backscattering coefficients extracted from RADARSAT image. *IEEE*

593   *Transactions on Geoscience and Remote Sensing, vol. 41: 1879 – 1888.*

594   **Shi, J., Wang, J., Hsu, A.Y., O'Neill, P.E., Engman, E.T. (1997).** Estimation of bare surface soil

595   moisture and surface roughness parameter using L band SAR image data. *IEEE Transactions on*

596   *Geoscience and Remote Sensing, vol. 35, n° 5: 1254–1266.*

597 **Singh, D. (2005).** A simplistic incidence angle approach to retrieve the soil moisture and surface

598 roughness at X-band. *IEEE Transactions on Geoscience and remote Sensing, vol. 43, n° 11:*

599 *2606-2611.*

600 **Srivastava, H.S., Patel, P., Manchanda, M.L., Adiga, S. (2003).** Use of multiincidence angle

601 RADARSAT-1 SAR data to incorporate the effect of surface roughness in soil moisture

602 estimation. *IEEE Transactions on Geoscience and Remote Sensing, vol. 41, n° 7: 1638–1640.*

603 **Srivastava, H.S., Patel, P., Navalgund, R.R., (2006).** Incorporating soil texture in soil moisture

604 estimation from extended low-1 beam mode RADARSAT-1 SAR data. *International Journal of*

605 *Remote Sensing, vol. 27, n°12-14: 2587– 2598.*

606 **Srivastava, H.S., Patel, P., Sharma, Y., Navalgund R.R. (2009).** Large area soil moisture

607 estimation using multi-incidence-angle RADARSAT-1 SAR data. IEEE Transactions on

608 Geoscience and Remote Sensing, vol. 47, n° 8: 2528–2535.

609 **Stolp, J., Janse, A.R.P. (1986).** X-band radar backscattering for detecting spatial distribution of

610 soil slaking. *ITC Journal, vol. 1: 82-87.*

611 **Taylor, G. R., Mah, H.A., Kruse, F.A., Kierein-Young, K.S., Hewson, R.D., & Bennett, B.A.**

612 **(1996).** Characterization of saline soils using airborne radar imagery. *Remote Sensing*

613 *Environment, vol. 57: 127 - 142.*

614 **Ulaby, F.T., Batlivala, P.P., & Dobson, M.C. (1978).** Microwave backscatter dependence on

615 surface roughness, soil moisture, and soil texture: Part I – Bare soil. *IEEE Transactions on*

616 *Geoscience and Remote Sensing, vol. GE-16, n° 4: 286-295.*

617 **Ulaby, F.T., Moore, R.K., & Fung, A.K. (1986).** Microwave Remote Sensing, Active and

618 Passive, From Theory to Applications, vol. 3, *Artech House, Inc., 685 Canton Street, Norwood,*

619 *MA 02062, 1098 p.*

620   **Valentin, C., Poesen, J., Li, Y. (2005).** Gully erosion: impacts, factors and control. *Catena vol.*

621   *63, n° 2–3: 132–153.*

622   **Valentin, C., & Bresson, L.M. (1992).** Morphology, genesis and classification of surface crusts in

623   loamy and sandy soils. *Geoderma, vol. 55: 225-245.*

624   **Wu, Q., Wang, M. (2007).** A framework for risk assessment on soil erosion by water using an

625   integrated and systematic approach. *Journal of hydrology, vol. 337: 11-21.*

626   **Zobeck, T.M., & Onstad, C.A. (1987).** Tillage and rainfall effects on random roughness*: a*

627   review. *Soil & Tillage Research, vol. 9: 1-20.*

628   **Zribi, M., Dechambre, M. (2002).** A new empirical model to retrieve soil moisture and roughness

629   from C-band radar data. *Remote Sensing of Environment, vol. 84: 42–52.*

630   **Zribi, M., Baghdadi, N., Holah, N., Fafin, O. (2005).** New methodology for soil surface

631   moisture estimation and its application to ENVISAT-ASAR multi-incidence data inversion.

632   *Remote Sensing of Environment, vol. 96: 485–496.*

633

Tables and Figures

633

634   *Table 1. Characteristics of TerraSAR images and in situ soil-moisture measurements.*

SAR acquisition date dd/mm/yy	Incidence angle	In situ soil moisture (%) [Min; Max]
17/03/09	25°	[24.7; 32.3]
18/03/09	50°	[24.5; 29.8]
25/03/09	50°	[24.1; 31.0]
26/03/09	25°	[23.9; 32.7]
08/04/09	25°	[16.8; 27.5]
09/04/09	50°	[15.2; 26.3]
17/04/09	25°	[14.1; 16.4]
20/04/09	50°	[18.3; 23.9]
11/05/09	25°	[25.8; 31.3]
01/03/10	50°	[33.4; 39.8]
02/03/10	25°	[32.7; 39.0]
04/03/10	25°	[27.3; 34.3]
12/03/10	50°	[12.6; 29.0]
13/03/10	25°	[14.9; 26.3]

635

636

637

638   *Table 2. Variations in soil moisture within the training plots (%). For each date and training plot,*

639   *the difference in soil moisture between soil II and soil I is shown. Slaking crust was observed on*

640   *soil II on March 17, 18, 25 and 26, 2009. N.A.: not available.*

Training plot ID	TerraSAR-X acquisition date (dd/mm/yy)								
	17/03/09 HH-25°	18/03/09 HH-50°	25/03/09 HH-50°	26/03/09 HH-25°	08/04/09 HH-25°	09/04/09 HH-50°	17/04/09 HH-25°	20/04/09 HH-50°	11/05/09 HH-25°
A	N.A.	N.A.	N.A.	N.A.	N.A.	N.A.	1.6	0.1	N.A.
B	N.A.	5.2	N.A.	2.7	0.5	1.4	0.9	0.2	0.2
C	4.7	3.7	0.5	-1.6	-1.4	-0.3	1.0	0.6	1.1
D	5.1	7.2	N.A.	1.0	N.A.	-1.4	0.1	0.4	0.4
E	3.1	2.9	0.2	-1.0	-0.4	0.1	0.1	0.7	N.A.
F	N.A.	N.A.	N.A.	N.A.	N.A.	N.A.	N.A.	N.A.	N.A.
G	N.A.	N.A.	N.A.	N.A.	N.A.	N.A.	0.7	0.9	0.1
Mean ($mv_{soil\ II}$ - $mv_{soil\ I}$) of training plots C, D, E	4.3	4.6	0.3	-0.5	-0.6	-0.5	0.4	0.6	0.7

641

642

643

644 *Table 3. Variations in the TerraSAR-X signal within the training plots (dB). For each date and*

645 *training plot, the difference between the radar signal of soil II and that of soil I is shown. Slaking*

646 *crust was observed on soil II on March 17, 18, 25, and 26, 2009. N.A.: not available.*

Training plot ID	TerraSAR-X acquisition date (dd/mm/yy)								
	17/03/09 HH-25°	18/03/09 HH-50°	25/03/09 HH-50°	26/03/09 HH-25°	08/04/09 HH-25°	09/04/09 HH-50°	17/04/09 HH-25°	20/04/09 HH-50°	11/05/09 HH-25°
A	1.6	1.5	0.5	0.8	0.3	-0.1	-0.2	0.1	1.4
B	2.7	2.1	-2.3	-0.7	0.6	-0.4	-0.5	0.5	-0.6
C	2.4	2.3	-0.1	-0.1	0.4	0.3	0.1	0.7	0.3
D	2.6	2.3	-1.1	0.1	0.7	0.8	-0.5	0.6	-0.2
E	2.8	2.3	-0.4	-0.2	0.8	1.3	N.A.	0.5	0.3
F	2.2	2.6	0.1	-0.4	0.7	0.8	-0.7	N.A.	1.2
G	1.1	1.1	-0.5	0.1	0.7	0.8	-0.1	0.9	0.1
Mean ($\sigma^\circ_{soil\,II} - \sigma^\circ_{soil\,I}$) of training plots C, D, E	2.6	2.3	-0.5	-0.1	0.6	0.8	-0.2	0.6	0.1

647

648

649

650

651 *Figure 1. Location of the Orgeval watershed (France; central coordinates: 48°51'N, 3°07'E).*
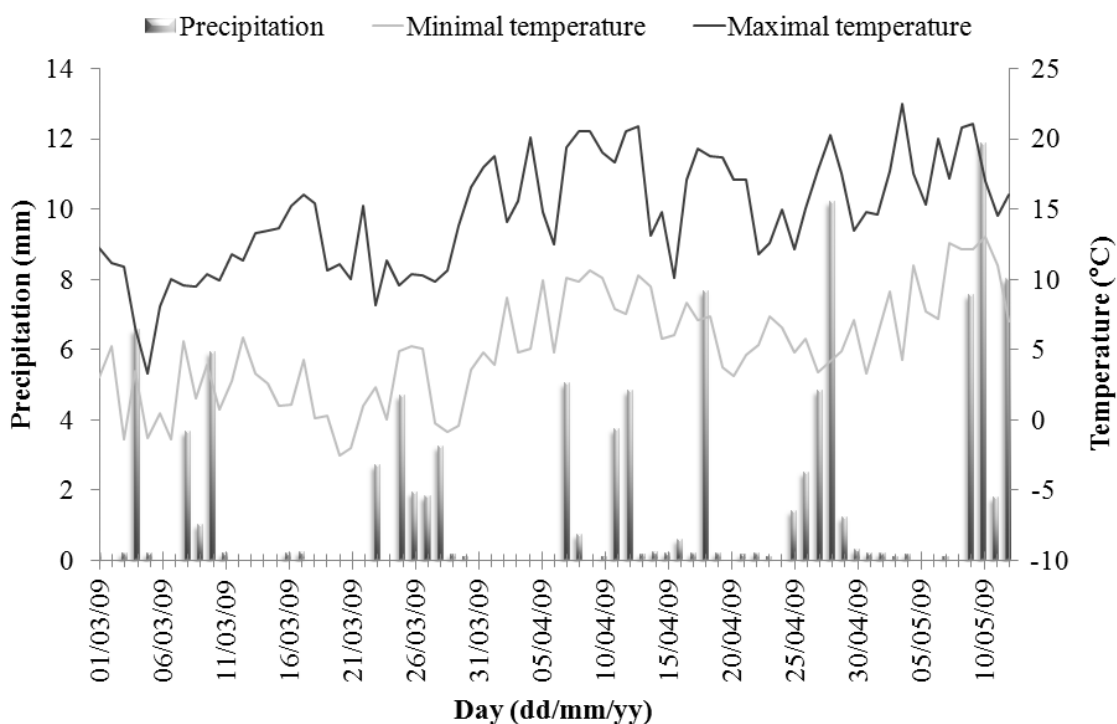
652

653

654 *Figure 2. A portion of a TerraSAR-X image (HH-25°, 17 March 2009) of the Orgeval site (central*

655 *coordinates: 48°52'N, 3°06'E). Field surveys were performed in seven plots (A to G) in 2009 and*

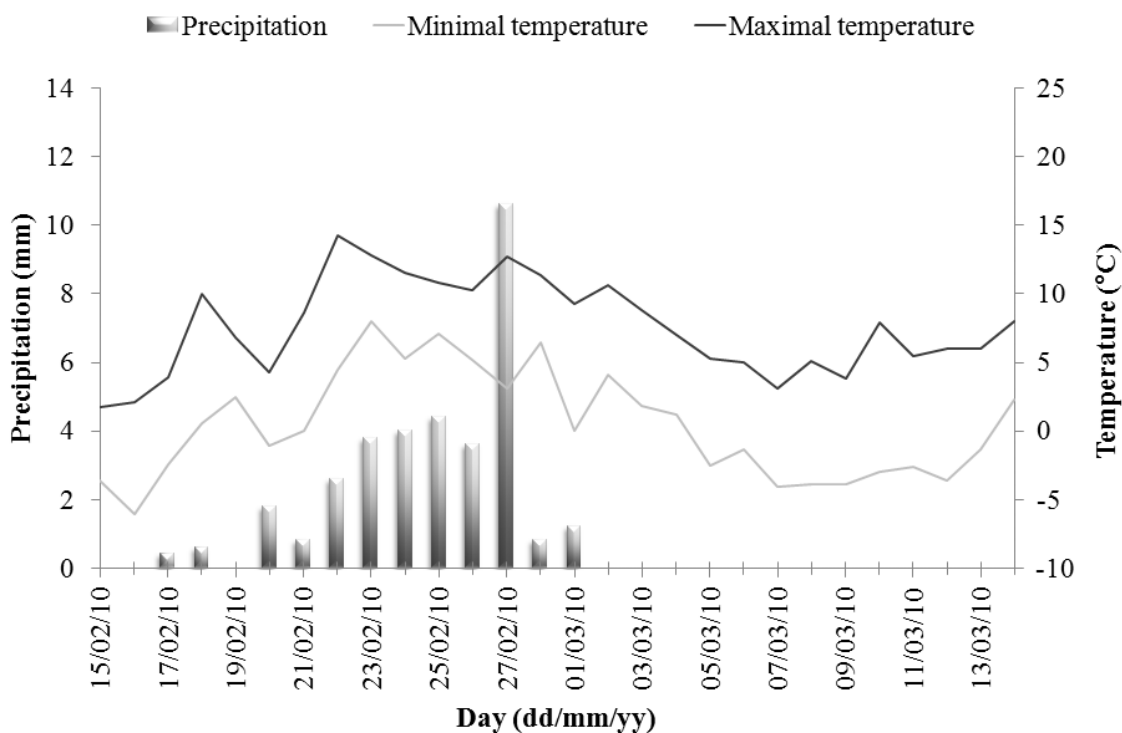656 *six plots (H to M) in 2010. The reference plots are outlined in black.*
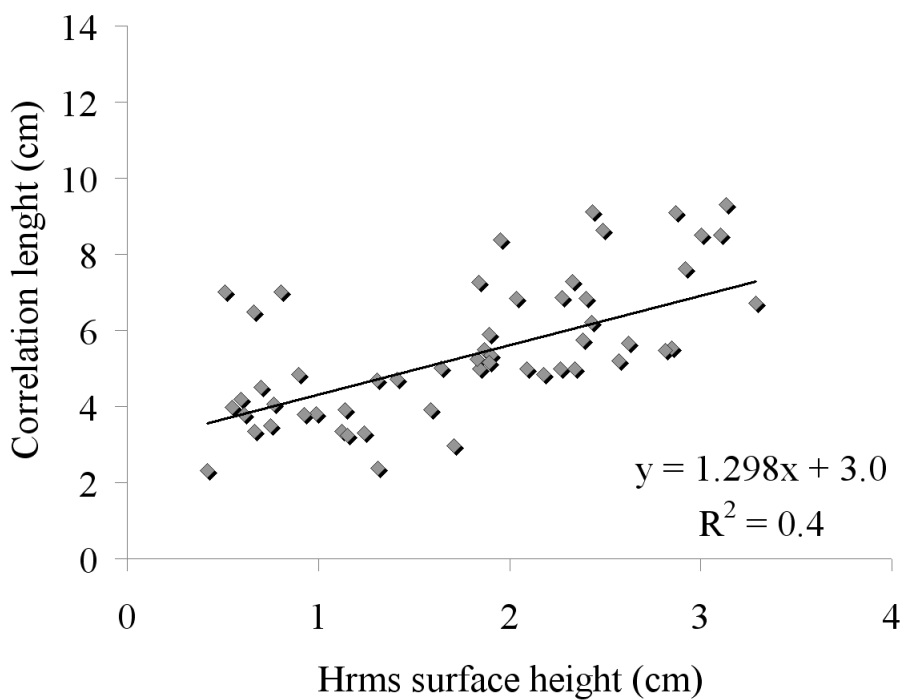
657

658

659

660

(a)

(b)

661

662   *Figure 3. Meteorological data averaged over the five stations installed in the basin: daily*

663   *precipitation (mm) and minimum and maximum temperatures in 2009 (a) and 2010 (b).*

664

The chart shows data points with a linear trend line. The y-axis is labeled "Correlation lenght (cm)" ranging from 0 to 14. The x-axis is labeled "Hrms surface height (cm)" ranging from 0 to 4.

$$y = 1.298x + 3.0$$
$$R^2 = 0.4$$

665   *Figure 4. Hrms surface height versus correlation length from measurements carried out in this*

666   *campaign.*

667

667
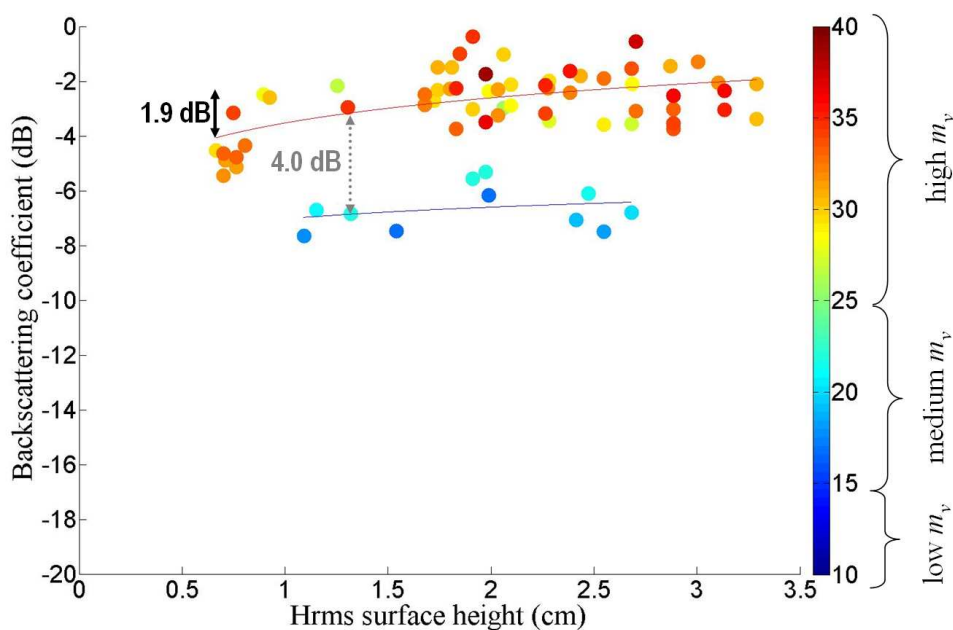
(a) medium *mv*: σ° = 0.62.ln(*Hrms*) - 7.0; R² = 0.1; RMSE = 0.7 cm
   high *mv*:   σ° = 1.32.ln(*Hrms*) - 3.5; R² = 0.3; RMSE = 0.9 cm
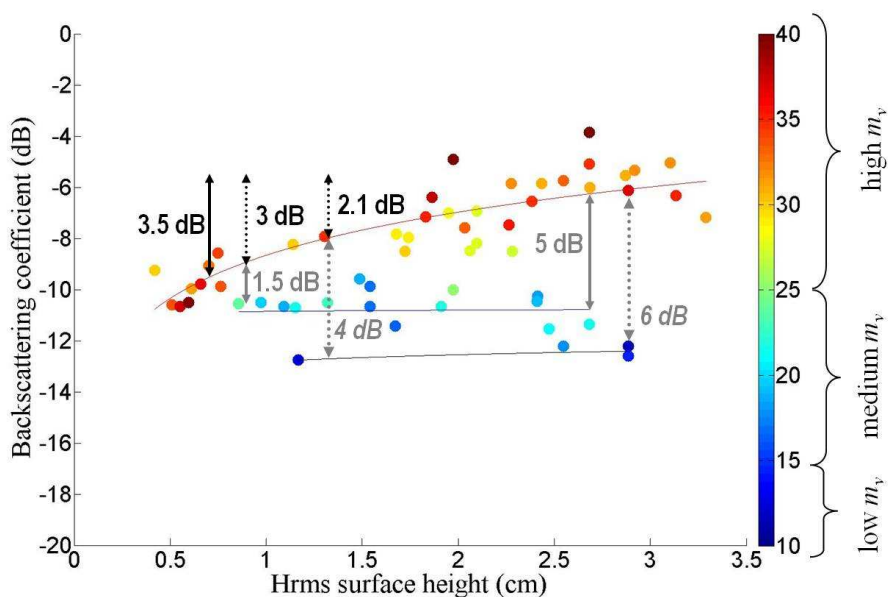
(b) low *mv*:   σ° = 0.20.ln(*Hrms*) - 12.9; R² = 0.5; RMSE = 0.1 cm
   medium *mv*: σ° = 0.01.ln(*Hrms*) - 10.3; R² = 0.1; RMSE = 0.6 cm
   high *mv*:   σ° = 2.43.ln(*Hrms*) - 08.7; R² = 0.7; RMSE =1.0 cm

668 *Figure 5. The sensitivity of the TerraSAR-X signal (at HH polarization) to soil roughness for*

669 *incidence angles of 25° (a) and 50° (b). Each point corresponds to one training plot (mean*
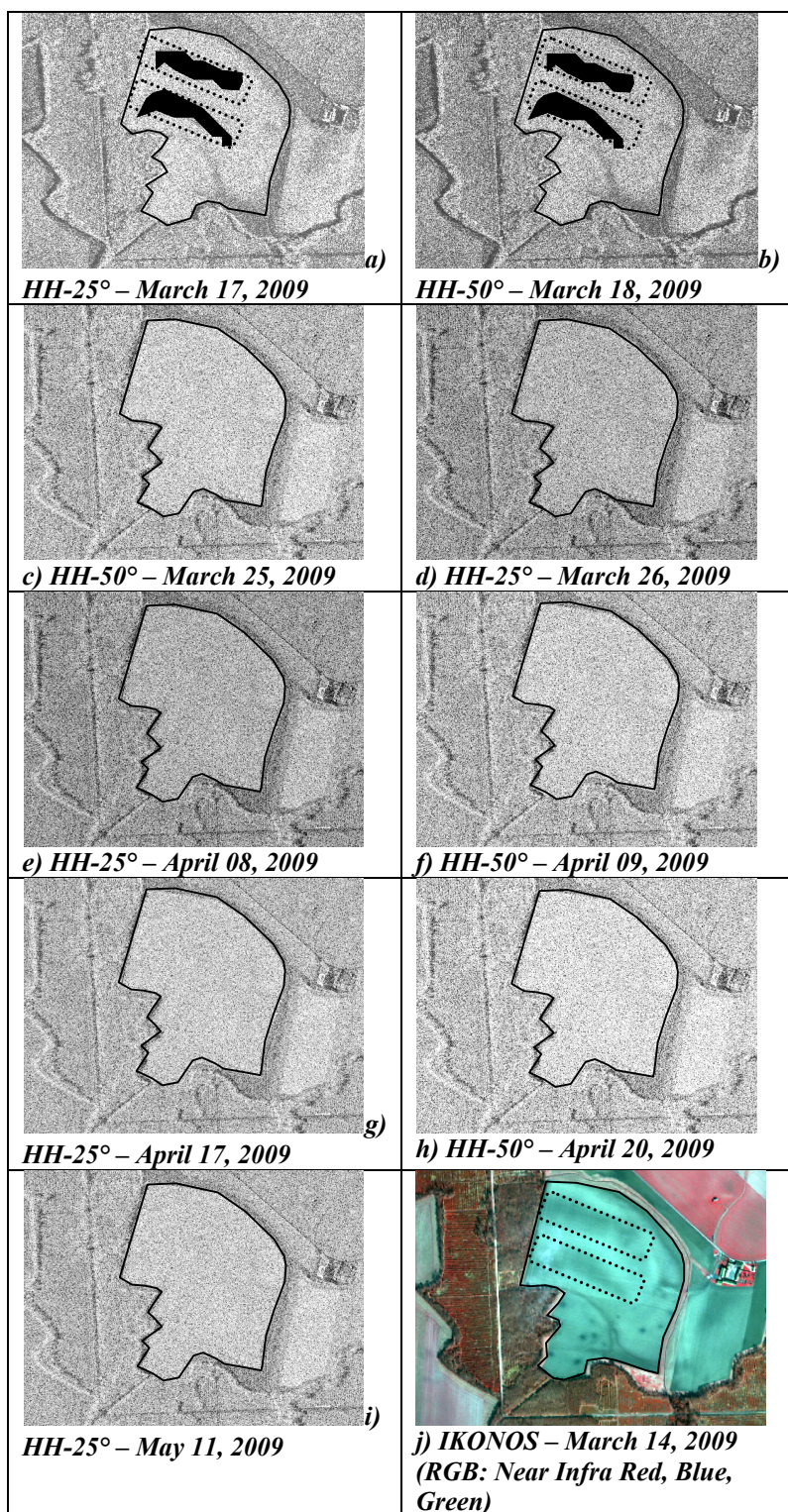
670 *values).*
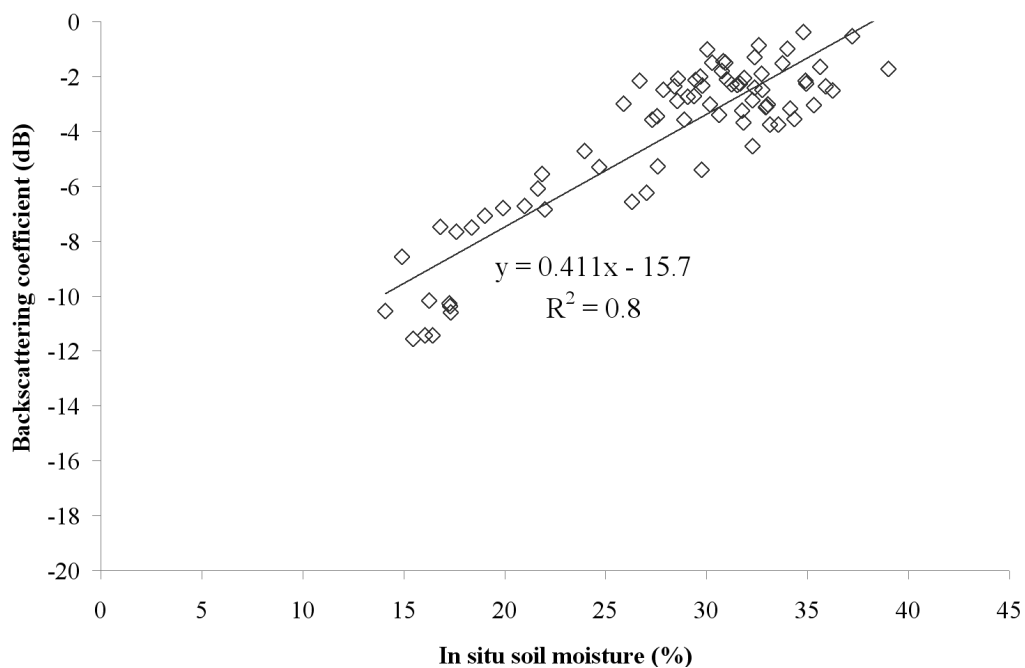
(a) RMSE =1.32%
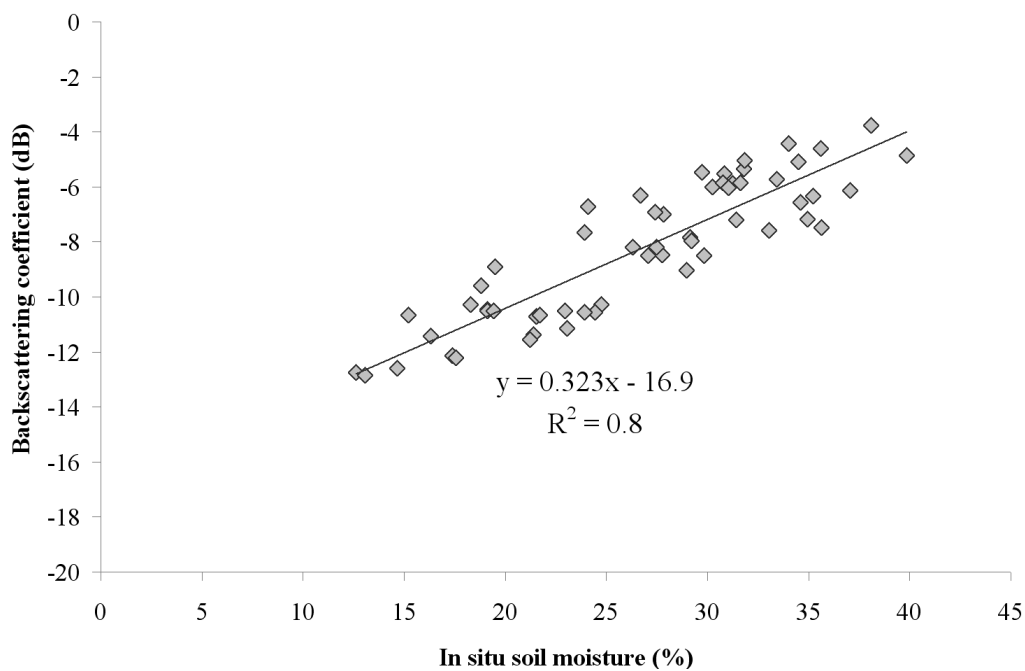
(b) RMSE =1.14%

671   *Figure 6. The sensitivity of the TerraSAR-X signal (at HH polarization) to soil moisture in the top*

672   *0–5-cm soil layer for incidence angles of 25° (a) and 50° (b). Each point corresponds to one*

673   *training plot or portion of a plot.*

Figure 7. Variations in signal strength within training plot C (outlined in black) for each

TerraSAR-X acquisition (a-i). A subset of the IKONOS image acquired on March 14, 2009 is also

shown (j). For the 17 and 18 March acquisitions, Soil I is outlined with a dotted black line (darker

zone), and soil II corresponds to the brighter zones.